



HAL
open science

Analysis of Homotypic Interactions of *Lactococcus lactis* Pili Using Single-Cell Force Spectroscopy

Ibrahima Dramé, Cécile Formosa-Dague, Marie-Pierre Chapot-Chartier,
Jean-Christophe Piard, Mickaël Castelain, Etienne Dague

► To cite this version:

Ibrahima Dramé, Cécile Formosa-Dague, Marie-Pierre Chapot-Chartier, Jean-Christophe Piard, Mickaël Castelain, et al.. Analysis of Homotypic Interactions of *Lactococcus lactis* Pili Using Single-Cell Force Spectroscopy. *ACS Applied Materials & Interfaces*, 2020, 12 (19), pp.21411-21423. 10.1021/ac-sami.0c03069 . hal-02860018

HAL Id: hal-02860018

<https://hal.inrae.fr/hal-02860018v1>

Submitted on 13 Jan 2022

HAL is a multi-disciplinary open access archive for the deposit and dissemination of scientific research documents, whether they are published or not. The documents may come from teaching and research institutions in France or abroad, or from public or private research centers.

L'archive ouverte pluridisciplinaire **HAL**, est destinée au dépôt et à la diffusion de documents scientifiques de niveau recherche, publiés ou non, émanant des établissements d'enseignement et de recherche français ou étrangers, des laboratoires publics ou privés.

Analysis of Homotypic Interactions of *Lactococcus lactis* Pili Using Single-Cell Force Spectroscopy

Ibrahima Dramé, Cécile Formosa-Dague, Christine Lafforgue, Marie-Pierre Chapot-Chartier, Jean-Christophe Piard, Mickaël Castelain, and Etienne Dague*



Cite This: <https://dx.doi.org/10.1021/acsami.0c03069>



Read Online

ACCESS |



Metrics & More

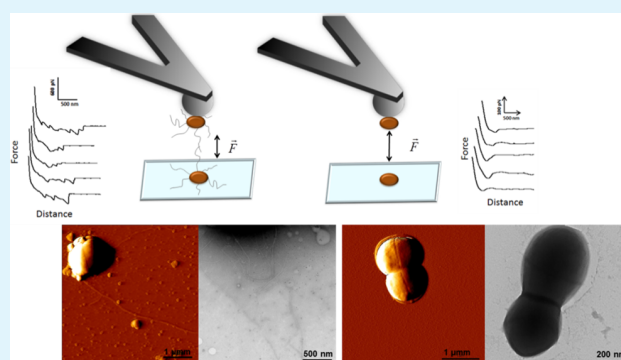


Article Recommendations



Supporting Information

ABSTRACT: Cell surface proteins of Gram-positive bacteria play crucial roles in their adhesion to abiotic and biotic surfaces. Pili are long and flexible proteinaceous filaments known to enhance bacterial initial adhesion. They promote surface colonization and are thus considered as essential factors in biofilm cohesion. Our hypothesis is that pili mediate interactions between cells and may thereby directly affect biofilm formation. In this study, we use single-cell force spectroscopy (SCFS) to quantify the force of the homotypic pili interactions between individual bacterial cells, using different *Lactococcus lactis* strains producing pili or not as model bacteria. Moreover the force–distance curves were analyzed to determine the physical and nanomechanical properties of *L. lactis* pili. The results for pili-devoided strains showed a weak adhesion between cells (adhesion forces and work in the range of 100 pN and 7×10^{-18} J, respectively). On the contrary, the piliated strains showed high adhesion levels with adhesion forces and adhesion work over 200 pN and 50×10^{-18} J, respectively. The force–extension curves showed multiple adhesion events, typical of the unfolding of macromolecules. These unfolding force peaks were fitted using the physical worm-like chain model to get fundamental knowledge on the pili nanomechanical properties. In addition, SCFS applied to a *L. lactis* isolate expressing both pili and mucus-binding protein at its surface and two derivative mutants revealed the capacity of pili to interact with other surface proteins including mucus-binding proteins. This study demonstrates that pili are involved in *L. lactis* homotypic interactions and thus can influence biofilm structuring.



KEYWORDS: *L. lactis*, biofilm, pili, SCFS, adhesion force, rupture length, adhesion work

INTRODUCTION

Pili (Latin for hairs) or fimbriae (Latin for threads) are proteinaceous filaments found at the surface of Gram-negative and positive bacteria. Several roles have been assigned to these proteinaceous structures particularly in the interactions of bacteria with their biotic or abiotic environment. They have been described to be involved in initial bacterial attachment to host tissues to mediate bacterial aggregation and to facilitate colonization and virulence of Gram-negative^{1–3} and Gram-positive pathogenic bacteria.^{4–7}

Pili in Gram-positive pathogens were first observed in *Corynebacterium renale*, a pathogenic bacterium responsible of pyelonephritis, using electron microscopy in the 1960s.⁸ However, while their existence has been known for several decades, their structure and mode of assembly have been characterized at the molecular level more recently.⁹ In contrast to pili of Gram-negative bacteria that are made of non-covalently bound pilins, pili of Gram-positive bacteria are made of pilin subunits that are covalently assembled by a transpeptidase named sortase C and the resulting polymer is

ultimately anchored by sortase A to peptidoglycan in the cell wall.¹⁰ Similar to what has been observed in Gram-negative bacteria, the presence of pili on the surface of Gram-positive pathogens has been long known to play a key role in the interaction with other proteins in the extracellular matrix, thereby influencing bacterial adhesion and the biofilm structure on biotic surfaces.^{6,11} Pili in nonpathogenic bacteria were discovered more recently in probiotic *Lactobacillus rhamnosus* GG,^{12–14} in commensal bifidobacteria,¹⁵ and also in the lactic acid bacterium (LAB) *Lactococcus lactis* present in various ecological niches such as plants and milk.¹⁶ In probiotic or commensal bacteria, pili could favor adhesion to the host intestinal mucosa and persistence in the gut. In regard

Received: February 17, 2020

Accepted: April 21, 2020

Published: April 21, 2020

to *L. lactis*, in the plant niche, pili could play a role in tissue colonization, while in dairy environment, they could interact with milk components. Moreover, piliated recombinant *L. lactis* might also be more effective to deliver therapeutic proteins in the gut.^{17–19}

L. lactis strains contain a chromosome-borne *pil* operon that encodes a putative sortase C (SrtC) as well as three putative pilins (PilA, PilB, and PilC). Pili formation was not observed in the laboratory strain *L. lactis* IL1403 under standard growth conditions; however, overexpression of the *pil* operon resulted in the synthesis of detectable pili structures (up to 3 μm in length with a diameter of 5 nm). PilB is the backbone of the pilus, covalently polymerized by the action of sortase C to form the filamentous structure of the pilus. PilA is the tip protein and PilC is the anchoring protein of the whole structure into the peptidoglycan layer. Mutants of the different proteins encoded by the *pil* operon from *L. lactis* IL1403 were then constructed to study the role of each pilus subunit in adhesion and biofilm formation. These investigations notably allowed to understand the role of pili in *L. lactis* adhesion to abiotic materials (polystyrene, stainless steel)²⁰ and in biofilm formation.¹⁶ The ability of piliated bacteria to stand on polystyrene under flow shear conditions was also studied, and the results showed that pili of *L. lactis*, and more particularly their backbones, were able to withstand a shear stress of more than 80 Pa, thereby showing their capacity to form strong adhesive bonds on abiotic surfaces.²⁰ In another study, optical tweezers were used to analyze the nanomechanical properties of single *L. lactis* pilus, which allowed to demonstrate that pili are highly flexible and inextensible structures.²¹ Finally, Oxaran et al.'s investigations¹⁶ demonstrated that pili of *L. lactis* are involved in the autoaggregation phenotype in liquid cultures and in the biofilm architecture, thus showing their crucial role in biofilm structuration and cell cohesion.

Pili were also characterized in a plant isolate of *L. lactis* (TIL448) with a backbone pilin (YhgE2) exhibiting 28% sequence similarity with PilB (YhgE) of *L. lactis* IL1403. In this strain, pili biosynthesis is encoded on a plasmid and assembly of pili was visualized without overexpression.²² These pili were shown to contribute to bacterial adhesion to epithelial cells and to mucins.^{22,23} During the 90s, AFM force spectroscopy has been developed to study, at the piconewton-scale, the interaction forces between individual molecules (ligand–receptor pairs, antibody–antigen, and complementary DNA strands).²⁴ More recently, single-cell force spectroscopy has been developed to measure intercellular and interbacterial interactions.²⁵ In example, the adhesion of *L. lactis* cells to pig gastric mucins has been investigated using this strategy and made it possible to decipher between the nonspecific and specific forces at play.²⁶ Regarding TIL448 and using AFM force spectroscopy, it was shown that both pili and a mucus-binding protein (Mub proteins) exposed at the bacterial surface contribute to adhesion of *L. lactis* TIL448 strains to mucins. Mub proteins are bacterial surface adhesins with typical signal peptide and C-terminal LPxTG, which contain multiple Mub domains (around 200 residues) and/or MucBP domains (around 50 residues).^{13,27,28} The comparative study of TIL448 and mutant derivatives expressing pili and Mub proteins or only pili or only Mub proteins enabled to elucidate the *L. lactis* muco-adhesive phenotype.²³ On AFM force–distance curves, showing the force recorded by the cantilever while it is approached and retracted from the surface, the authors observed rupture events both at short (100 to 200 nm)

and long distances (up to 600–800 nm) that they attributed, respectively, to Mub proteins and pili unfolding.²⁹ Moreover, the role of pili and Mub proteins in adhesion was investigated under shear stress conditions on the mucin layer.²³ The results of these experiments showed a more important contribution of the Mub protein compared to pili for the adhesion to the mucin layer.

In the process of biofilm formation, the interactions between cells are of first importance. In this intercellular adhesion, several kinds of molecules among which pili may play a crucial role³⁰ in the cohesion of cells in biofilm formation.

In the work presented here, the objective was to analyze homotypic interactions between pili at the single-molecule scale. To reach this goal we used an advanced AFM technique called single-cell force spectroscopy (SCFS) to probe the interactions between pili present on the surfaces of two individual bacteria, thereby allowing to characterize the nanomechanical properties of the pili–pili bond for *L. lactis* cells expressing more or less pili. The specificity of homotypic interactions was verified by monitoring the pili–pili interactions in the presence of anti-PilB antibodies. The rupture peaks observed on the obtained force curves were then described by the worm-like chain (WLC) model. The results unravelled the role of *L. lactis* pili in homotypic interactions of laboratory strain IL1403 mutants. Experiments conducted on the vegetal isolate TIL448 expressing both pili and Mub proteins further demonstrate the capacity of pili to interact with other surface proteins including Mub proteins. These findings are valuable to understand the influence of pili on adhesion, structuring, and cohesion of the cells during biofilm formation.

MATERIALS AND METHODS

Bacterial Strains and Growth Conditions. Bacterial strains derived from *L. lactis* subsp. *lactis* used in this study are described in Table 1. Strains were grown in M17 broth (Oxoid) containing 0.5%

Table 1. *L. lactis* Strains Used in this Study

strains	genotype or phenotype	source/reference
VE17061	Pil ⁻ , control (pili minus)	16
VE17173	Pil ⁺ , over expression of the <i>pil</i> operon	16
VE17176	Pil ⁺⁺ , over expression of both the <i>pil</i> operon and the <i>srtA</i> gene	16
TIL448	Pil ⁺ /Mub ⁺ , vegetal strain isolated from peas	22
TIL1230	Pil ⁻ /Mub ⁻ , TIL448 derivative obtained by plasmid curing	22
TIL1289	Pil ⁻ /Mub ⁺ , TIL448 derivative obtained by disruption of the <i>yhgE2</i> gene encoding the backbone pilin, Ery ^R	22
TIL1290	Pil ⁺ Mub ⁻ , TIL448 derivative obtained by disruption of the <i>mub</i> gene encoding a mucus-binding protein, Ery ^R	22

(w/v) D-glucose (M17 Glc). When required, antibiotics were added to the medium to a final concentration of 5 $\mu\text{g}/\text{mL}$ for erythromycin (Ery) and tetracycline (Tet). The strains were incubated overnight at 30 °C under static conditions.

Bacterial Sample Preparation for AFM Measurements. Overnight cultures were obtained by inoculating 500 μL of a cell suspension from frozen stock in 10 mL of medium. Cultures were harvested by centrifugation (1000 g, 10 min, at room temperature). The cell pellet was resuspended in phosphate-buffer saline (PBS 1X) solution at pH 7.4 and then diluted up to an optical density of 0.02 at 600 nm to obtain isolated cells. These cells were then immobilized on dopamine-coated glass coverslips. Briefly, glass coverslips were

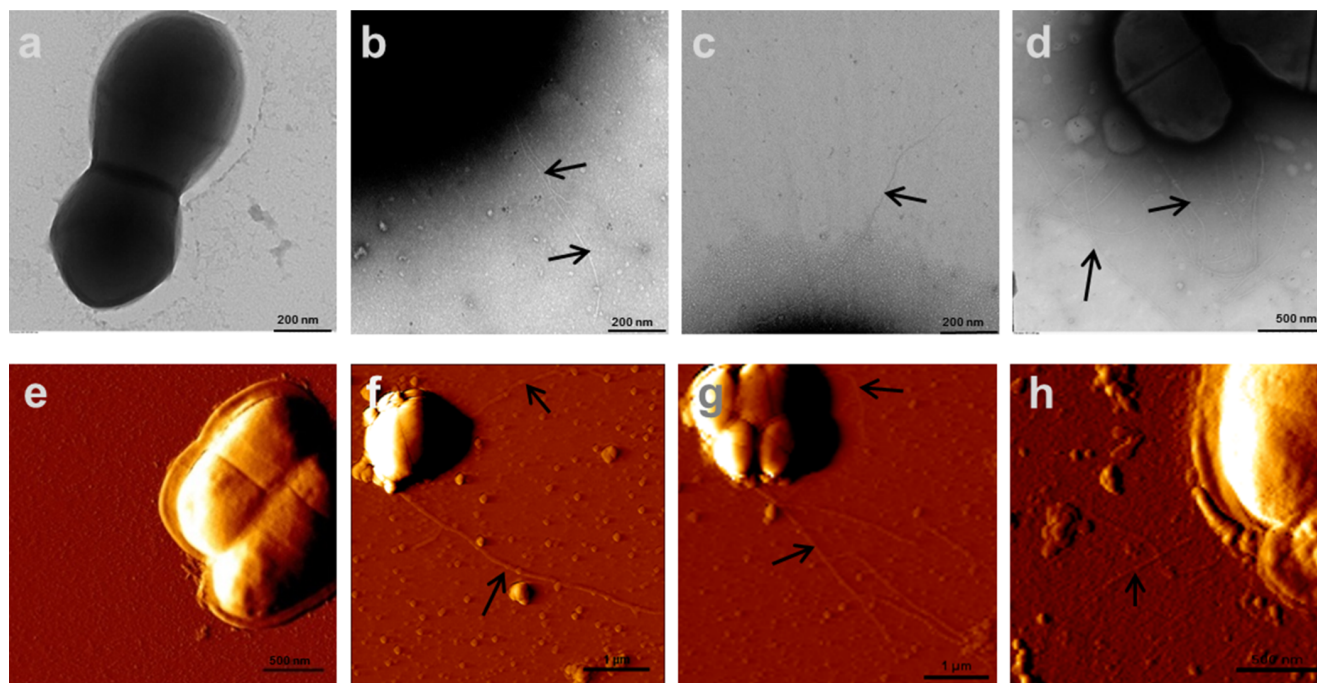


Figure 1. TEM and AFM images of *L. lactis* pili. TEM images obtained after negative staining of (a) control Pil⁻ VE17061, (b) Pil⁺ VE17173, (c) Pil⁺⁺ VE17176, and (d) Pil⁺/Mub⁺ TIL448 strains. AFM contact imaging in air of (e) Pil⁻ VE17061, (f) Pil⁺ VE17173, (g) Pil⁺⁺ VE17176, and (h) Pil⁺ Mub⁺ TIL448 strains. The pili are indicated on the images by the black arrows.

cleaned for 5 min using oxygen plasma and immersed for 48 h in a PBS 1X solution containing 4 mg/mL of dopamine hydrochloride (99%, Sigma). They were then rinsed in Milli-Q-grade water and ethanol and dried under nitrogen. A total of 50 μ L of the diluted bacterial suspension was then applied to the dopamine-coated glass coverslip, allowed to stand for 30 min at room temperature, and directly used for AFM single-cell force spectroscopy (SCFS) experiments.

AFM Single-Cell Force Spectroscopy Experiments. Cell probes were prepared using the protocol described in Beaussart et al. Briefly, colloidal probes were obtained by attaching a single silica microsphere (5 μ m diameter, Bangs Laboratories) with a thin layer of UV-curable glue (NOA 63, Norland Edmund Optics) on triangular tipless cantilevers (NP-O10, Bruker, USA) and using a Nanowizard III AFM (Bruker USA). Cantilevers were then immersed for 1 h in PBS 1X containing 4 mg/mL of dopamine hydrochloride (Sigma-Aldrich), rinsed in PBS 1X, and used directly for cell probe preparation. The nominal spring constant of the colloidal probe cantilever was ranging from 0.03 to 0.06 N/m, as determined by the thermal noise method.³¹ The colloidal probe was then brought into contact with an isolated bacterium and retracted to attach the bacterial cell. Proper attachment of the cell on the colloidal probe was checked using optical microscopy. Cell probes were used to measure cell–cell interaction forces at room temperature, using a maximum applied force of 1 nN, a constant approach retraction speed of 2.0 μ m/s, and a contact time of 0.5 s. Data were analyzed using the Data Processing software from JPK Instruments (Bruker, USA). Adhesion force and work of adhesion histograms were obtained by calculating the maximum adhesion force and the area under the retract curve, respectively, for each force curve obtained. Unless stated otherwise, for each condition, experiments were repeated for three bacteria coming from independent cultures.

AFM Imaging of *L. lactis* Pili. Bacteria were grown overnight at 30 °C under static conditions. The following day, 50 μ L of the cell suspension was diluted in 5 mL of PBS 1X. A drop of 50 μ L of the diluted cell suspension was then immobilized on freshly cleaved mica surfaces and incubated at 30 °C for 3 h. The mica surfaces were then rinsed three times in Milli-Q water, and the samples were dried in an

incubator at 30 °C for 2 h. Surface topography images of dried bacteria were recorded using AFM in contact mode in air at room temperature, using MLCT cantilevers (Bruker, USA, nominal spring constant of \sim 0.01 N/m, as determined using the thermal noise method) with a scanning rate of 1 line/s and a resolution of 512 \times 512 lines.

Transmission Electron Microscopy of *L. lactis* Pili. To check for the presence of pili on the surface of *L. lactis* strains used in this study, transmission electron microscopy (TEM) and a negative staining procedure were used. Bacterial suspensions from overnight cultures were harvested by centrifugation (1000 g, 10 min at room temperature) and washed in PBS 1X. Bacterial cells were then fixed using paraformaldehyde (PFA) 3% during 30 min at room temperature. Formvar carbon-coated copper grids were rinsed in a drop of fixed bacteria and allowed to stand for 3 min for the bacterial cells to adsorb over the material. Staining was performed in uranyl acetate (0.2%) during 20 s after washing the grids in Milli-Q water. The grids were dried using a Whatman grad cellulose filter paper. Samples were observed at 75 kV with an H-600 TEM (Hitachi, Japan) equipped with a 1024 \times 1024 pixel format orca CCD camera. Result images were treated using imageJ software.

RESULTS

Visualization of Pili in Different *L. lactis* Strains. As a first step, we checked for the absence/presence of pili at the surface of different *L. lactis* strains (Table 1) in our growth conditions, using both transmission electron microscopy (TEM) (representative images: Figure 1a–d) and AFM contact imaging in air (representative images: Figure 1e–h). As expected, both TEM micrographs and AFM images showed pili exhibiting filamentous structures at the surface of cells from strains VE17173 (Figure 1b,f), VE17176 (Figure 1c,g), and TIL448 (Figure 1d), referred to as Pil⁺, Pil⁺⁺, and Pil⁺ Mub⁺, respectively. As expected, no pili were observed at the surface of cells from the Pil⁻ VE17061 control strain (Figure 1a,e). Higher numbers of pili were detected in the Pil⁺⁺ VE17176 strain than in the Pil⁺ VE17173 strain, consistent with previous

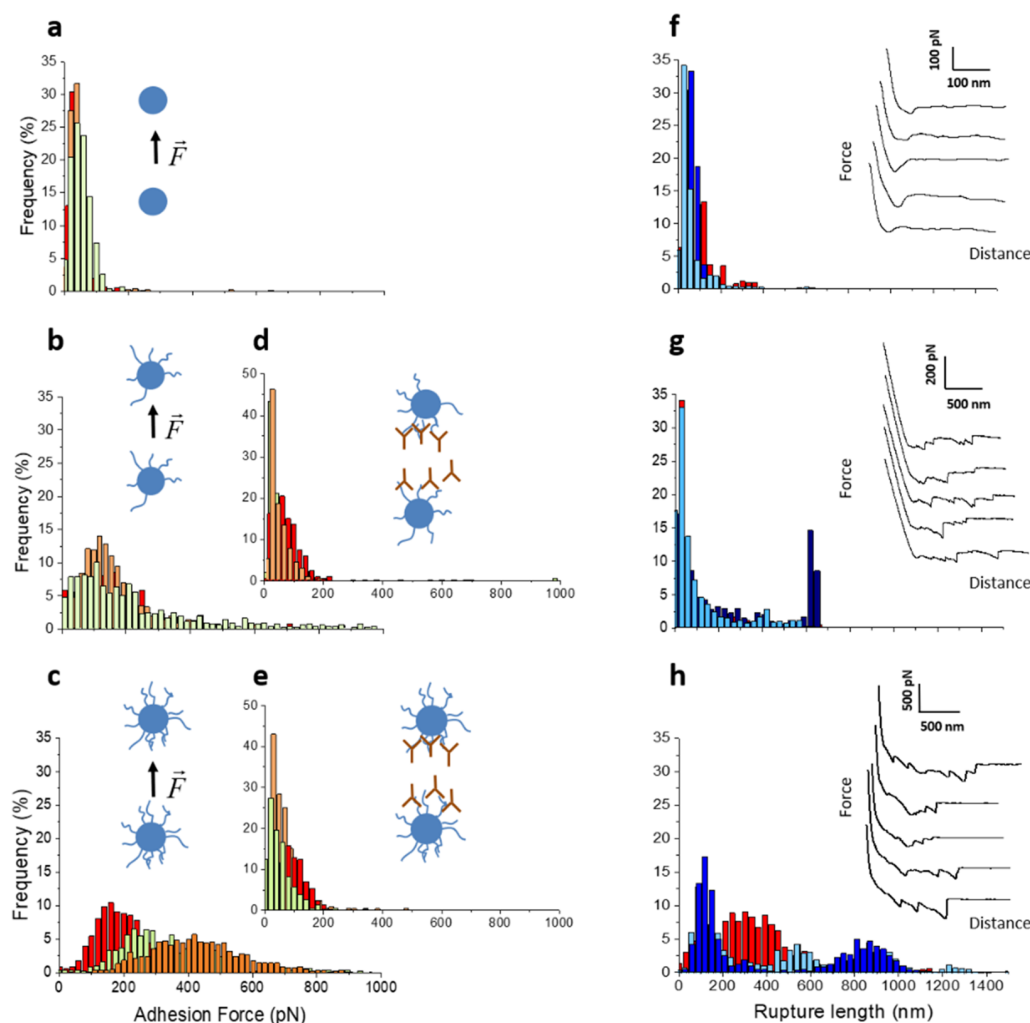


Figure 2. *L. lactis* pili mediate homotypic interactions between cells. Pili–pili interactions are measured between cell pairs of individual bacteria using single-cell force spectroscopy. Histograms representing the (a–e) adhesion force, (f–h) rupture lengths, and typical retraction force curves, obtained by recording force curves between cells of (a, f) the Pil[−] control VE17061, (b, g) the Pil⁺ VE17173, and (c, h) the Pil⁺⁺ VE17176 strains were reported. For each strain, three independent experiments were conducted (one experiment means three pairs (corresponding to the three colors) of independent cells). The results presented here relate to one experiment and were representative of the three experiments (the two others are presented in Figure S3: homotypic interactions between the Pil[−] VE17061 cells, Figure S4: homotypic interactions between the Pil⁺ VE17173 cells, and Figure S5: homotypic interactions between the Pil⁺⁺ VE17176 cells). The total number of analyzed force curves per strain was above 3000 and above 1000 for each histogram. Force measurements performed in the presence of anti-YhgE antibodies in (d) the Pil⁺ VE17173 and (e) the Pil⁺⁺ VE17176 strains were reported. $n > 1000$ for three pairs cells, representative of three experiments.

western blot analyses in which the former produced greater amounts of oligomerized pilins than the latter.¹⁶ In Figure 1, the pili are indicated by the black arrows. In the Pil⁺ VE17173 strain, the lengths measured were ranging from 200 to 4400 nm and in average 1178 ± 1074 nm. The Pil⁺⁺ VE17176 and the Pil⁺ Mub⁺ TIL448 strains showed pili lengths between 250 to 4100 nm and 600 to 5500 nm, respectively. The average lengths were 1424 ± 1012 nm for the Pil⁺⁺ VE17176 strain and 2930 ± 1884 nm for the Pil⁺ Mub⁺ TIL448 strain. As shown in Figure 1c,d,g, pili were tangled and extremely thin with width ranging from 5.22 to 9.32 nm and the average was 6.7 ± 1.3 nm.

Cell–Cell Interactions Are Dominantly Mediated by Pili. Then, in the second step, our goal was to characterize, at the molecular level, the homotypic interactions between pili from different *L. lactis* strains used in this study (Table 1). For this purpose, we used single-cell force spectroscopy

(SCFS),^{32,32,33} as described in the Materials and Methods section. The adhesion force measurements recorded between pairs of cells from each strain type are presented in Figure 2. It showed the result of typical force curve analyses obtained for three cells pairs (three different colors) coming from one culture (the results from two other cultures are presented in Figures S3: homotypic interactions between the Pil[−] VE17061 cells, Figure S4: homotypic interactions between the Pil⁺ VE17173 cells, and Figure S5: homotypic interactions between the Pil⁺⁺ VE17176 cells). For each force curve, the adhesion force (Figure 2a–c), rupture length (Figure 2e–g), and adhesion work values (Figure 3a–c) were extracted. The quantification of the adhesion frequency (19.1% of adhesive curves) showed that the Pil[−] VE17061 control strain cells that do not display pili adhered weakly to each other with adhesion forces in the range of 47 ± 30 pN (mean \pm SD; total number of force curves = 1225 from three different cell pairs) and an

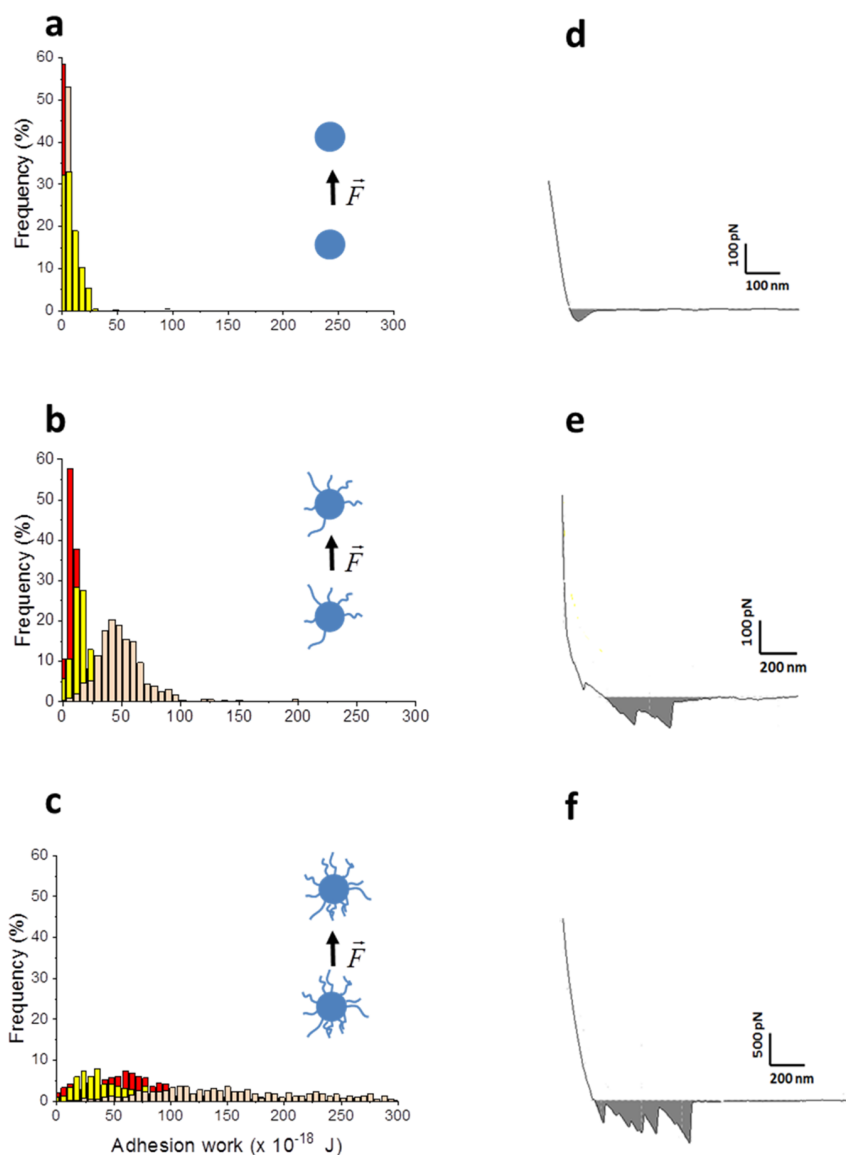


Figure 3. Role of pili–pili homotypic interactions in *L. lactis*–*L. lactis* adhesion work. Frequency histograms and typical force distance curves showing the adhesion work observed for (a) the Pil[−] VE17061 control strain, (b) the Pil⁺ VE17173, and (c) the Pil⁺ VE17176 strains. The adhesion work is expressed in joule ($\times 10^{-18}$ J) and is determined by measuring the area under the force–distance curves as exemplified on panels (d–f). For each strain, three independent experiments were conducted (one experiment means three pairs of independent cells).

average rupture distance of 52 ± 40 nm. In pilated strains, higher adhesion frequencies were found, i.e., 78.0% in Pil⁺ VE17173 and 90.1% in Pil⁺ VE17176 strains. The adhesion forces ranged from 150 ± 60 to 198 ± 99 pN (mean \pm SD; total number of force curves = 1817 from three different cell pairs) for the Pil⁺ VE17173 strain and from 182 ± 75 to 452 ± 150 pN (mean \pm SD; total number of force curves = 2914 from three different cell pairs) for the Pil⁺ strain. As for the rupture lengths, they reached 634 ± 103 nm for the Pil⁺ VE17173 strain and 874 ± 147 nm for the Pil⁺ VE17176 strain. Force curves recorded for pilated strains showed multiple adhesive events that were absent in the Pil[−] VE17061 control strain suggesting that they were related to pili–pili interaction (see below). To further investigate this point, we performed several control tests in which we probed the interactions between pilated and pili-devoided control strain cells (Supporting Information, Figure S1: heterotypic interaction between Pil⁺ VE17173 and Pil[−] VE17061). This showed

a weak adhesion force (73 ± 47 pN) similar to the interaction between cell pairs of the control strain. Moreover, other control tests were performed to study the specificity of pili–pili interactions. To go one step further in the probing of pili–pili interactions, we reasoned that because the pilus backbone is constituted of oligomers of the YhgE pilin and because these oligomers have been shown to be the essential determinant for the adhesion of pilated cells under shear flow conditions,²⁰ anti-YhgE antibodies¹⁶ should be able to block pilus–pilus interactions. As reported in Figure 2d,e, major reductions in the adhesion force (24.1 ± 11.6 to 64.8 ± 43.8 pN for the Pil⁺ VE17173 strain and 31.4 ± 22.5 to 75.2 ± 55.3 pN for the Pil⁺ VE17176 strain) were monitored thus proving that the interactions probed were indeed due to interactions between YhgE pilins.

To further probe the homotypic interactions between pili, we determined the work of adhesion involved. The adhesion work was calculated as the area between the retract force curve

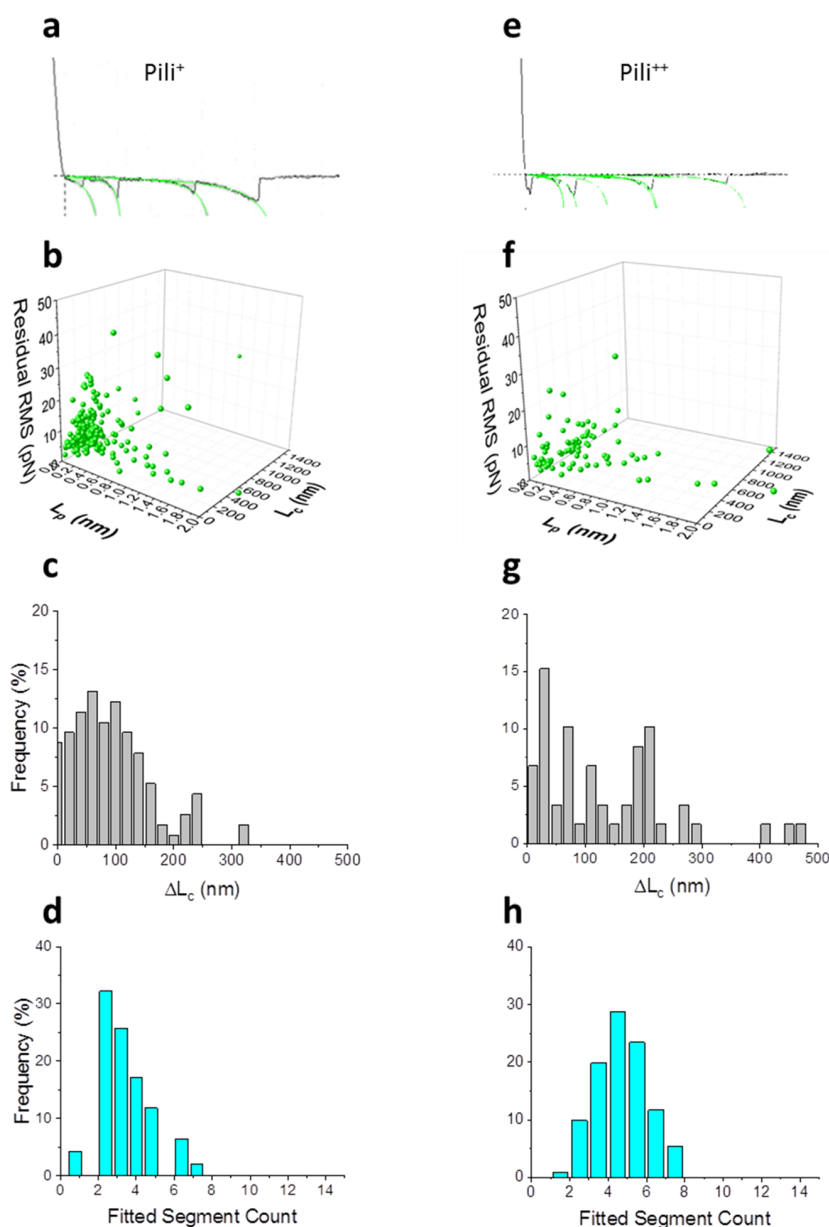


Figure 4. Pili–pili homotypic interaction: analysis of the force signature. Unfolding curves were fitted using the worm-like chain model (WLC). (a, e) Typical unfolding curves (black lines) respectively from the Pil⁺ VE17173 and Pil⁺⁺ VE17176 strains and typical fits (green lines). The contour length (L_c), persistence length (L_p), and RMS residual relations are presented in (b) and (f). The distance between (c, g) two consecutive ruptures (ΔL_c) and (d, h) the number of fitted segment per curve respectively from the Pil⁺ VE17173 and the Pil⁺⁺ VE17176 strains were analyzed.

and the baseline of this force curve, as illustrated in Figure 3d–f. The results presented in Figure 3a–c showed that interactions between cells of piliated strains engage an important energy, ranging from $15 \times 10^{-18} \pm 7$ to $47 \times 10^{-18} \pm 15$ joule (J) for the Pil⁺ cells and up to $108 \times 10^{-18} \pm 27$ J for the Pil⁺⁺ ones, compared to the Pil⁻ control strain that engages only $7 \times 10^{-18} \pm 0.5$ J. These values indicate stronger interactions between piliated cells and suggest that pili play a crucial role in adhesion of cell to cells.

Force Curve Signatures Description Using the Worm-like Chain (WLC) Model. To understand, at the physical level, the different force peaks observed during the extension of a pilus–pilus complex (or pili–pili complex) (Figure 2e–g), we used the WLC model. The WLC model is commonly used to describe the force–extension response of linear polymers

that undergo thermal fluctuations. This model is usually used to describe macromolecule extension and is expressed in the following equation:^{34–36}

$$F(x) = -k_b T / L_p [1/4(1 - x/L_c) - 2 + x/L_c - 1/4]$$

where F is the force (N), k_b is the Boltzmann constant (J/Kelvin), T is the temperature (Kelvin), L_p is the persistence length (m), L_c is the total contour length (m) of the macromolecule, and x is the molecule extension (m). Other conformational parameters were determined such as the distance between two consecutive ruptures (ΔL_c) (Figure 4c,g), the number of fitted segment per force curve (Figure 4d,h), and the fitting quality, evaluated by the residual Root Mean Square (residual RMS) values. The fitting of typical unfolding force curves (Figure 4a,e) respectively from the Pil⁺

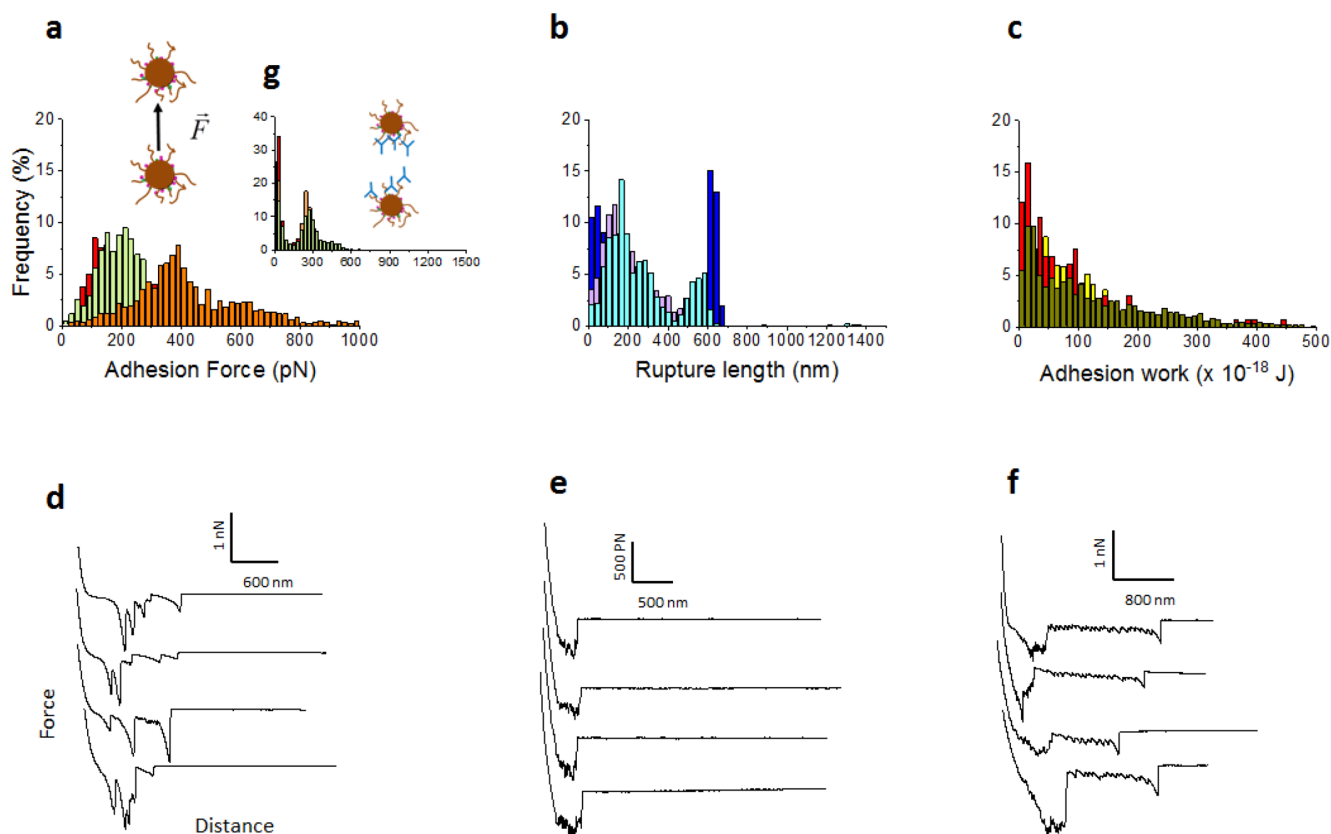


Figure 5. Cell–cell interactions of the plant isolate *L. lactis* TIL448 involve pili–pili homotypic interactions and more complex interactions. (a–c) Histograms of the adhesion force, rupture length, and adhesion work of the self-interaction of TIL448, respectively. (d–f) Representative of the three types of force curves recorded for this self-interaction. Force curves of three pairs of cells, representing three independent experiments, have been analyzed ($n > 1000$). Force measurements were also performed in the presence of anti-YhgE, and the histogram frequency of the adhesion force is represented in (g) ($n > 1000$).

VE17173 ($n = 92$) and the Pil⁺⁺ VE17176 strains ($n = 50$) were analyzed. The frequency distribution of L_c , L_p , and residual RMS values are presented on 3D graphs in Figure 4b,f. The L_p values obtained for both the Pil⁺ VE17173 and the Pil⁺⁺ VE17176 strains were in between 0.05 and 0.6 nm and reach 1 nm at maximum. The L_c values were variable and ranged from 50 to 800 nm for the Pil⁺ VE17173 strain and from 100 to 1000 nm for the Pil⁺⁺ VE17176 strain. The fit parameters were those providing the lowest RMS values, or in other words, those providing the best quality of the fit. We found the smallest residual RMS when L_p and L_c were freely adjustable parameters. Indeed, the residual RMS on L_p and L_c for the Pil⁺ VE17173 strain or the Pil⁺⁺ VE17176 strain were found to be 3 and 6.7 pN, respectively, in the case of freely adjustable parameters, and increased up to 379 pN in the case of an L_p value fixed to 0.4 nm (Supporting Information, Figure S10: analysis of various force signatures obtained in pili–pili interactions between the Pil⁺⁺ VE17176 cells and Figure S11: analysis of various force signatures obtained in pili–pili interactions in Pil⁺ Mub⁺ TIL448 strains).

In these conditions, we found ΔL_c values between 25 and 200 nm and three to four unfolding events (corresponding to the number of interacting pili) for the Pil⁺ VE17173 strain (Figure 4c,d). As for the Pil⁺⁺ VE17176 strain, the ΔL_c values ranged from 25 to 300 nm (Figure 4g) and the numbers of fitted segment were of 5 to 6 (Figure 4h). These values of L_p (which are small, i.e., in the range of 0.05 to 0.6 nm), L_c (up to 800 nm), and ΔL_c (up to 300 nm) measured in both Pil⁺

VE17173 and Pil⁺⁺ VE17176 strains indicate that pili are long, rigid, but flexible biopolymers. This results in long range interactions between cells that are hydrodynamically stable.²⁰ The interactions exhibited, randomly, different lengths, as it can also be seen in the microscopic images (Figure 1).

Cell–Cell Interactions in a Plant Isolate *L. lactis* TIL448. In order to strengthen the above conclusions, we decided to challenge our results obtained with engineered laboratory strains by comparing them with those obtained in an environmental strain that naturally produces pili (TIL448). To reach this goal, we studied the interactions between two TIL448 cells. *L. lactis* TIL448 not only produces pili but also produces Mub proteins known for their adhesive properties to mucin layers. Using SCFS experiments, the adhesion between individual cell pairs was measured with three independent cell pairs (Figure 5) showing large adhesion forces ranging from 197 ± 83 to 372 ± 82 pN ($n = 3795$ force curves in Figure 5a) on almost all the recorded force curves (the adhesion frequency is 97.9%). The rupture length was as high as 627 ± 21 nm (Figure 5b) and could reach 1.2 μm (shown in Figure S6: homotypic interactions between the Pil⁺ Mub⁺ TIL448 cells). These values, in addition to the adhesion work values over $50 \times 10^{-18} \pm 16$ J (Figure 5c), were of the same order of magnitude to that of the adhesion frequency, force, rupture distance, and work obtained with the laboratory pilated strains (Pil⁺ and Pil⁺⁺). To challenge the importance of pili in the interactions measured, we once again performed the blocking test by adding anti-YhgE antibody in the solution; this

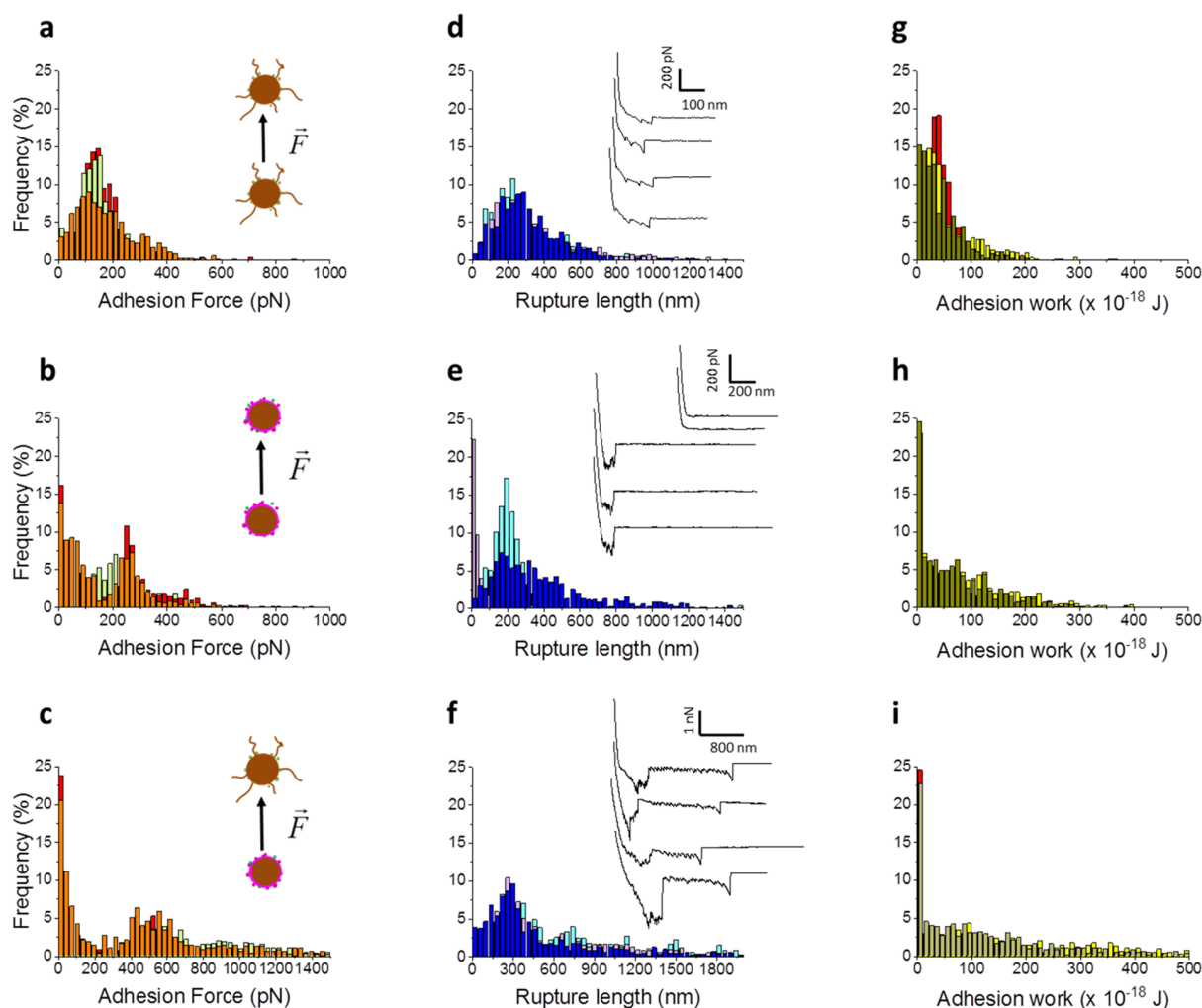


Figure 6. Analysis of cell–cell interactions on mutants from TIL448. (a–c) Adhesion frequency, (d–f) rupture distance and typical force distance curves, and (g, h, i) adhesion work were measured between cell pairs of (a, d, f) $\text{Pil}^+ \text{Mub}^- \text{TIL 1290}$, (b, e, h) cell pairs of $\text{Pil}^- \text{Mub}^+ \text{TIL 1289}$, and heteropairs of TIL1290 with TIL1289. Each condition has been tested three times with three pairs using cells coming from independent cultures. The results presented here are coming from three pairs, representative of the three independently performed experiments. The other two cultures are in Figure S7: homotypic interactions between $\text{Pil}^+ \text{Mub}^- \text{TIL 1290}$ cells, Figure S8: homotypic interactions between $\text{Pil}^- \text{Mub}^+ \text{TIL 1289}$ cells, and Figure S9: heterotypic interactions between $\text{Pil}^+ \text{Mub}^- \text{TIL 1290}$ and $\text{Pil}^- \text{Mub}^+ \text{TIL 1289}$ cells.

resulted in a dramatic decrease in the adhesion rate to only 30.3% (Figure 5g).

By taking a closer look at the force curves obtained, we were able to decipher three different classes of signatures (examples showed in Figure 5d–f) indicating different types of interaction modes probably resulting from different molecules interacting with each others at the surface of TIL448 cells.

To identify the nature of these different interacting proteins and their correspondence to the typical force curves observed in Figure 5d–f, we used three TIL448 strain derivatives (Table 1): $\text{Pil}^+ \text{Mub}^- \text{TIL 1290}$, $\text{Pil}^- \text{Mub}^+ \text{TIL 1289}$, and $\text{Pil}^- \text{Mub}^- \text{TIL 1230}$. Using these strains, we analyzed both homotypic interactions for each strain and heterotypic interactions taking place between the $\text{Pil}^+ \text{Mub}^- \text{TIL 1290}$ strain and $\text{Pil}^- \text{Mub}^+ \text{TIL 1289}$ strain.

In the $\text{Pil}^+ \text{Mub}^- \text{TIL 1290}$ strain, cell–cell interactions showed that the adhesion force, rupture length, and adhesion work were 130 ± 55 pN, 255 ± 138 nm, and $39 \times 10^{-18} \pm 11$ J, respectively, for 89.7% of the force curves (Figure 6a,d,g) (mean \pm SD; total number of force curves = 1319 and from

three different cell pairs). The other two cultures are in Figure S7: homotypic interactions between $\text{Pil}^+ \text{Mub}^- \text{TIL 1290}$ cells. The force curve shape between $\text{Pil}^+ \text{Mub}^- \text{TIL 1290}$ cells was very similar to those obtained above with the Pil^+ and Pil^{++} strains (Figure 2f,g), indicating that the pili–pili interactions had a specific force signature corresponding to Figures 4a,e, 5d, or 6d). For the $\text{Pil}^- \text{Mub}^+ \text{TIL 1289}$ strain, we observed both a high level of nonadhesive events (63.4%) and a high adhesion force (36.6% of curves) of 255 ± 23 pN (Figure 6b). The rupture length (Figure 6e) was measured to be 202.0 ± 0.2 nm and most of the cells (63.4% of force curves) showed low energy ($9.1 \times 10^{-18} \pm 10.4$ J), while a high energy ($38.8 \times 10^{-18} \pm 17$ J) was observed for only 36.6% of force curves (Figure 6h). The force curve signatures presenting a sawtooth-shaped pattern are comparable to those observed in Figure 5e corresponding to Mub protein unfolding. The interaction between the $\text{Pil}^+ \text{Mub}^- \text{TIL 1290}$ and $\text{Pil}^- \text{Mub}^+ \text{TIL 1289}$ cells ($n = 2227$ force curves) (Figure 6c,f,i) showed nonadhesive frequency for 55.9% of the force curves and only 44.1% present a high adhesion force (559 ± 165 pN) and work of adhesion

Table 2. Summary Table of Results^a

strains	Pil/Mub	adhesion frequency (%)	adhesion force (pN)	rupture distance (nm)	adhesion work ($\times 10^{-18}$ J)	L_c (nm)	L_p (nm)	ΔL_c (nm)	number of fitted segments	RMS (pN)
VE17061	-/-	19.1	47 \pm 30	52 \pm 40	7 \pm 0.5	nd	nd	nd	nd	nd
VE17173	+/-	78.0	150 \pm 60 to 198 \pm 99	reach 634 \pm 103	15 \pm 7 to 47 \pm 15	50 to 800	0.05 to 0.6	25 to 200	3 to 4	6.7
VE17176	++/-	90.1	182 \pm 75 to 452 \pm 150	874 \pm 147	up to 108 \pm 27	100 to 1000	0.05 to 0.6	25 to 300	5 to 6	3.0
TIL448	+/+	97.9	197 \pm 83 to 372 \pm 82	up to 627 \pm 21	over 50 \pm 16	nd	nd	nd	nd	nd
TIL1230	-/-	16.8	29 \pm 16	59 \pm 32	5.3 \pm 1.5	nd	nd	nd	nd	nd
TIL1289	-/+	36.6	255 \pm 23	202 \pm 0.2	38.8 \pm 17	200 to 600	0.051	50	8 to 10	20.0
TIL1290	+/-	89.7	130 \pm 55	255 \pm 138	39.1 \pm 11	200 to 1200	0.05 to 0.15	25 to 250	12 to 18	6.7
TIL1290/ TIL1289	+/-, -/+	44.1	559 \pm 165	up to 1500 \pm 95	131 \pm 125	300 to 1500	until 0.2	50	12 to 18	10.0

^and = not determined.

(131 $\times 10^{-18}$ \pm 125 J). The rupture length was up to 1500 \pm 95 nm. The analysis of the different force curves shows three different profile types. Among the adhesive curves, some showed typical Mub protein unfoldings while others were similar to those observed in Figure 5f and included the detachment of Mub protein before the sliding of pili on the Mub protein. The hypothesis is that several Mub proteins on the cell surface act as adhesins along the pili. The force applied on the pili then results in successive detachment of Mub–pili interactions, which we called sliding and was also described as zipper interactions in *L. rhamnosus* GG.¹⁴

Finally, and as expected, the Pil⁻ Mub⁻ TIL1230 strain showed a dramatic decrease in the adhesion force, distance rupture, and adhesion work to 29 \pm 16 pN, 59 \pm 32 nm, and 5.3 $\times 10^{-18}$ \pm 1.5 J, respectively (Supporting Information, Figure S2: homotypic interaction in TIL1230).

To facilitate the comparison between strains, the results concerning the adhesion, force and work, rupture distance, adhesion frequency, etc., are gathered in a recapitulative table (Table 2).

Description of Various Force Signatures in the Plant Isolate *L. lactis* TIL448. Similar to piliated derivatives from IL1403 strains (Table 1), the different force peaks obtained in TIL448 cell interactions were well described by the WLC model. The typical force curves for pili (Figure 7a) and Mub protein (Figure 7e) unfolding and the signatures resulting of the sliding of pili to Mub proteins (Figure 7i) were analyzed. For pili signatures, as shown in Figure 7b, the L_p values were between 0.05 to 0.15 nm, the L_c values were from 200 to 1200 nm, and the ΔL_c were variable (between 25 to 250 nm) (Figure 7c). The number of fitted segment varied between 2 and 6 (Figure 7d). These values were similar to those found with the laboratory IL1403 piliated strains. Figure 7f shows that the L_p and L_c values of Mub protein unfolding (sawtooth signatures) were more homogeneous and about 0.051 nm and from 200 to 600 nm, respectively. The ΔL_c value was fixed at 50 nm (Figure 7g) and the number of fitted segments from 8 to 10 (Figure 7h). The ΔL_c value was also at 50 nm (Figure 7k) when we analyzed the peak obtained by the pili sliding on Mub proteins (sawtooth signatures and the last corresponds to the pili detachment, Figure 7i). The L_p was up to 0.2 nm, the L_c was between 300 to 1500 nm (Figure 7j), depending on the length of the pili sliding on the Mub proteins. The number of fitted segments was 12 to 18 (Figure 7l). All the fits had

residual RMS values below 20 pN demonstrating the good fitting quality compared to the values obtained when we fixed L_p to one value (Supporting Information, Figure S12: analysis of various force signatures of Mub proteins obtained in the interactions between the Pil⁻ Mub⁺ TIL1289 cells, Figure S13: analysis of various force signatures obtained in the interactions between the Pil⁺ Mub⁻ TIL1290 and the Pil⁻ Mub⁺ TIL1289 cells).

DISCUSSION

For several decades, most of the investigations on pili were conducted in pathogens because of their role in colonization, infection, and virulence.^{1,4,37} It was only recently that pili were also evidenced and characterized in food and probiotic bacteria such as *L. lactis* or *Lactobacillus rhamnosus* GG.¹³ In this study, we raised the question of the pili function in the group of lactic acid bacteria (LAB).

LAB were natural inhabitants of agricultural products such as plants and milk and they were used as starters in a number of food fermentation processes. As such, LAB were likely to occur as biofilms on various food (processing) surfaces and host mucosal cells.^{38,39} In this regard, the role of pili in mucin and collagen binding, the two major extracellular components of host epithelial layers, have been extensively investigated in *L. rhamnosus*.¹⁴ Further, single-cell approaches were used to probe interactions of LAB cells through their surface proteins, in order to understand biofilm formation in positive or detrimental situations.

In laboratory strains, the results showed that piliated strains reached an adhesion force of \sim 600 pN while it was less than 100 pN for control cells. These results suggested that pili are involved in the interactions between cell pairs. In addition, we observed a difference in adhesion force between cell pairs from the same culture and between Pil⁺ and Pil⁺⁺ bacteria suggesting that (i) the number of pili at the bacterial surface is not constant and (ii) the number of pili can influence the adhesion abilities. To clear this point, we performed several control experiments including the one presented in Figure S1: heterotypic interaction between Pil⁺ VE17173 and Pil⁻ VE17061. This revealed weak adhesion force and work combined with short rupture length, clearly demonstrating that such interactions have no role in cell–cell interactions. To further validate the direct implication of homotypic interactions of pili in cell–cell interactions, we used anti-YhgE

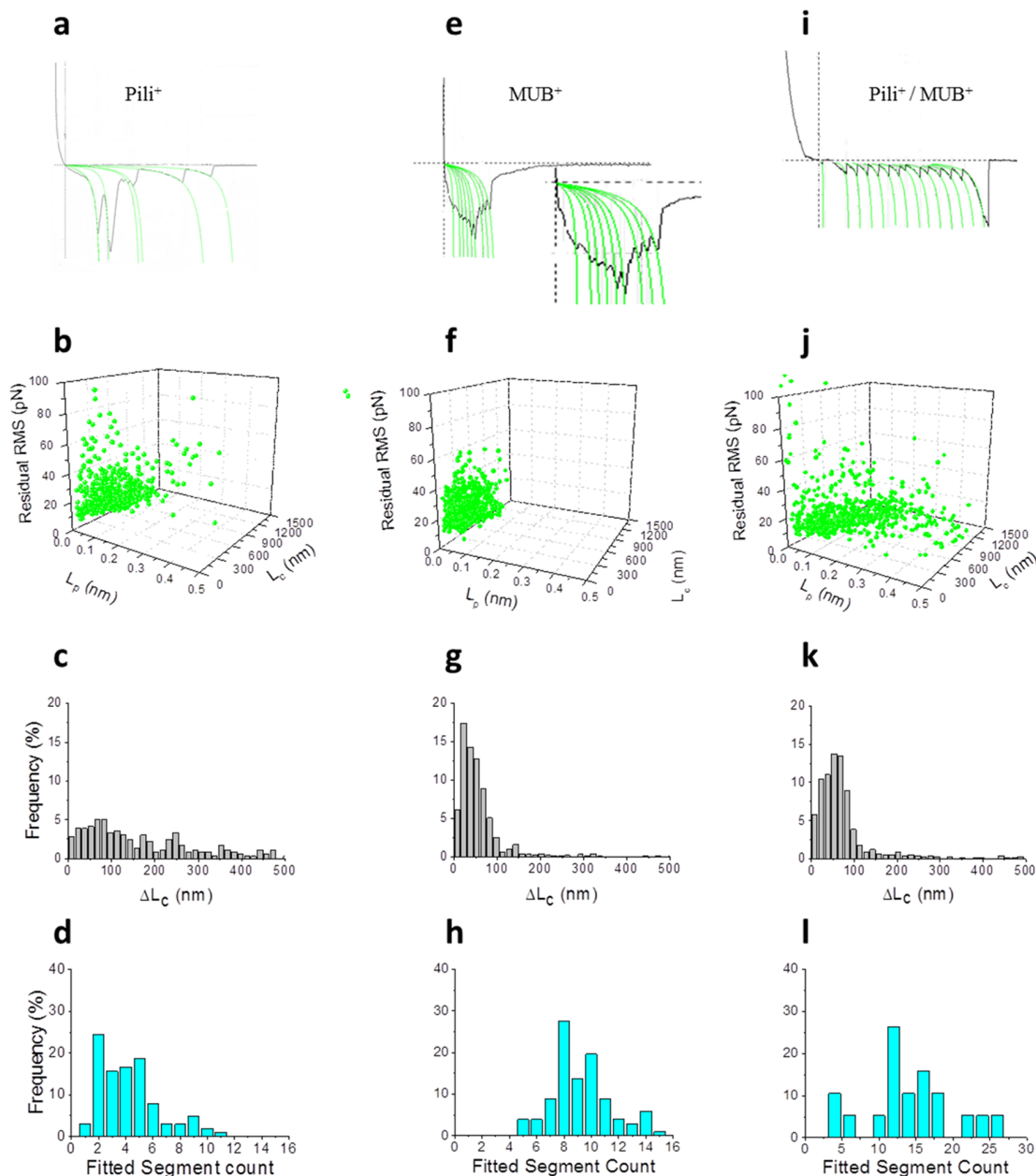


Figure 7. Physical analysis of various force signatures obtained in homotypic interactions for the vegetal isolate TIL448 and its derivatives. Typical unfolding curves from (a) Pil⁺ Mub⁺ and (e) Pil⁻ Mub⁺ (i) were fitted (green lines) with the WLC model. The fitting of 100 typical force curves was made, and the persistence length (L_p), contour length (L_c), and residual RMS are represented in (b), (f), and (j), respectively. (c, g, k) Distance between two consecutive rupture (ΔL_c) and (d, h, l) number of fitted segment per curve were analyzed.

antibodies to block the pili–pili interactions. Blocking pili–pili interactions with anti-YhgE antibodies resulted in a major reduction in adhesion forces, work, and distance rupture, thus showing the central role of the pili backbone (YhgE or PilB) in the homotypic interaction. The histograms of the blocking experiment in TIL448 (inset in Figure 5g) were similar to the interactions between Pil⁻ Mub⁺ TIL1289 cells (Figure 6b) or between Pil⁺ Mub⁻ TIL1290 and Pil⁻ Mub⁺ TIL1289 cells (Figure 6c). These observations demonstrated the implication of pili in homotypic cell–cell interactions in both laboratory and environmental strains. This was consistent with a previous report focused on the specific interactions between small adhesins along the pili of *L. rhamnosus* GG.¹⁴ Indeed, the authors in this study concluded that pili have multisite

attachment and may have an important functional role in strengthening bacterial–bacterial interactions in the intestinal environment.

Another interesting parameter to better describe the role and function of pili homotypic interactions in cell–cell adhesion was the work of adhesion. The low values measured for control strains (less than 10×10^{-18} J) were in line with those found by Wang et al.⁴⁰ in control cells of *Klebsiella pneumoniae*, a Gram-negative bacteria, able to produce type 3 fimbriae (pili-like). In this study, the adhesion work was 17×10^{-18} to 19×10^{-18} J for type 3 fimbriae-producing bacteria and 11×10^{-18} J in the fimbriae-deficient strain. These values were in the same order of magnitude with those obtained here in the Pil⁻, Pil⁺, and Pil⁺⁺ strains ($7 \times 10^{-18} \pm 0.5$ J, $15 \times 10^{-18} \pm 7$ to $47 \times$

$10^{-18} \pm 15$ J, and up to $108 \times 10^{-18} \pm 27$ J, respectively). These congruent values illustrate favorable interactions between piliated cells and suggest that pili play a crucial role in cell–cell adhesion. This was consistent with previous observations of the tight aggregation phenotype of piliated *L. lactis* cells in liquid culture and with the structuration of piliated lactococci biofilms.¹⁶

The analysis of rupture event distances (Figure 2f,g and Figure 6d) showed the existence of short and long distances (up to 1500 ± 95 nm), which were coherent with the differences in pili length observed in the images presented in Figure 1. The force signatures of pili from *L. lactis* strains were different from those described in *L. rhamnosus* GG, which showed sawtooth patterns composed of multiple small force peaks corresponding to the detachment of small adhesins along the pili.¹⁴ However, in the environmental Pil⁺ Mub⁺ TIL448 strain, no adhesins along the pili were found (Figures 5d and 6d), but sawtooth patterns, due to the sliding of the pili on Mub proteins, were observed. These Mub proteins do not interact with each other (data not shown) but rather with other components of the cell surface or other surface proteins including pilins. The sliding of pili on Mub proteins was observed in retraction profiles and showed sawtooth patterns (Figures 5f and 6f). This confirms the interaction between pili and Mub proteins. The interactions between pili and other surface proteins, such as milk proteins, were also demonstrated in *L. rhamnosus* GG^{14,41,42} and can be related to the better ability of these strains to form biofilms and interact with the proteins of the extracellular matrix.

The unfolding of both the pili–pili and pili–Mub interactions were described by the WLC model, which has often been used to analyze the unfolding of polypeptidic molecules. In this model, the unfolded macromolecule was considered as an irregular curved filament, which was linear at the scale of the persistence length L_p . In addition to L_p , other parameters such as contour length L_c and ΔL_c were also extracted from the data. L_c is the length of the fully extended molecule and ΔL_c is the distance in between each unfolding peak. L_p , L_c , and ΔL_c were key parameters to describe and to understand the unfolding profiles that were obtained. The L_p values ranged from 0.05 to 0.6 nm, which is close to the values found by Lu et al. on type IV pili in *Pseudomonas aeruginosa* PAO1 ($L_p = \sim 0.8$ nm) and to the L_p values found by Fahs et al.⁴³ (0.02 to 0.7 nm) for the pili of *L. rhamnosus* GG. These two studies both used the same physical model as we did (WLC model). Fahs et al.⁴³ and Guerin et al.⁴² explained that the low values of L_p were related to a weak potential of deformation. This means that pili were most probably rigid structures. Our data were in line with these interpretations that were also confirmed by Castelain et al.²¹ in their study of pili using optical tweezers. Moreover, Miller et al.⁴⁴ also showed that the low value of the L_p meant that the globular subunit of PilB was not unfolded but that the pili polypeptidic chain was stretched.⁴⁴ The variability of the L_c values (between 50–1500 nm) showed that pili were made of macromolecules of different lengths. L_c reflects the distance between two cells when the pili–pili interaction vanished.⁴⁵ The differences in L_c values can be explained by the variation in the number of polymerized monomers (100 to 200 monomers¹⁶) that form the backbone of the pili. Our result for L_c were comparable with the values obtained by Rheinlaender et al.⁴⁶ with the pili of *Corynebacterium diphtheria*. Using the WLC model, these authors measured dispersed L_c , ranging from 260 to 1590 nm.

This could be due to random locations of the interactions between pili resulting in unfoldings of random lengths.⁴³ This interpretation was confirmed by our ΔL_c analysis, which actually showed multimodal distribution (between 25–200 nm, Figures 4c,g and 7c).

CONCLUSIONS

SCFS is a powerful technique to quantify the adhesion behavior between individual bacteria. Using this technique, we demonstrated in this work that in *L. lactis*, cell–cell adhesion abilities were driven by the presence of pili on their surface. In addition, both laboratory and environmental *L. lactis* showed a high adhesion force and work, in the case of piliated strains. This allowed us to demonstrate that pili–pili interactions were specific and homotypic. Based on the sawtooth signatures obtained when pili interact with Mub proteins, we assume that along the pili, there are several binding sites for proteins but there are no adhesins. This behavior of pili helped to understand the cell–cell adhesion step of biofilm formation and thus their influence on cell cohesion and biofilm structuring. From the nanomechanical point of view, the low L_p and variable L_c values, in addition to the observation of pili by TEM and AFM imaging, showed that pili of *L. lactis* were rigid and possessed a highly flexible polypeptide chain. The ability of LAB such as *L. lactis* cells to interact with each others through pili could be further used in medical applications such as mucosal vaccines or therapeutic drug delivery. In the industrial environment, the understanding of the pili–pili interactions and their role in the cell–cell adhesion step of biofilm formation could be useful to use positive biofilms in order to control proliferative undesired species.

ASSOCIATED CONTENT

Supporting Information

The Supporting Information is available free of charge at <https://pubs.acs.org/doi/10.1021/acsami.0c03069>.

Heterotypic interactions between Pil⁺ VE17173 and Pil[−] VE17061; homotypic interactions between TIL1230 cells; interactions between Pil[−] VE17061 cells, cultures 2 and 3; homotypic interactions between Pil⁺ VE17173 cells, cultures 2 and 3; homotypic interactions between Pil⁺⁺ VE17176 cells, cultures 2 and 3; homotypic interactions between Pil⁺ Mub⁺ TIL448 cells, cultures 2 and 3; homotypic interactions between Pil⁺ Mub[−] TIL1290 cells, cultures 2 and 3; homotypic interactions between Pil[−] Mub⁺ TIL1289 cells, cultures 2 and 3; heterotypic interactions between Pil⁺ Mub[−] TIL1290 and Pil[−] Mub⁺ TIL1289 cells, cultures 2 and 3; analysis of various force signatures obtained in pili–pili interactions between the Pil⁺⁺ VE17176 cells; analysis of various force signatures obtained in pili–pili interactions in Pil⁺ Mub⁺ TIL448 strains; analysis of various force signatures of Mub proteins obtained in the interactions between the Pil[−] Mub⁺ TIL1289 cells; and analysis of various force signatures obtained in the interactions between the Pil⁺ Mub[−] TIL1290 and the Pil[−] Mub⁺ TIL1289 cells (PDF)

AUTHOR INFORMATION

Corresponding Author

Etienne Dague – LAAS-CNRS, Université de Toulouse, CNRS, 31000 Toulouse, France; orcid.org/0000-0003-3290-9166; Email: edague@laas.fr

Authors

Ibrahima Dramé – TBI, Université de Toulouse, INSA, INRAE, CNRS, 31000 Toulouse, France; LAAS-CNRS, Université de Toulouse, CNRS, 31000 Toulouse, France

Cécile Formosa-Dague – TBI, Université de Toulouse, INSA, INRAE, CNRS, 31000 Toulouse, France; orcid.org/0000-0002-8627-3784

Christine Lafforgue – TBI, Université de Toulouse, INSA, INRAE, CNRS, 31000 Toulouse, France

Marie-Pierre Chapot-Chartier – Université Paris-Saclay, INRAE, AgroParisTech, Micalis Institute, 78350 Jouy-en-Josas, France

Jean-Christophe Piard – Université Paris-Saclay, INRAE, AgroParisTech, Micalis Institute, 78350 Jouy-en-Josas, France

Mickaël Castelain – TBI, Université de Toulouse, INSA, INRAE, CNRS, 31000 Toulouse, France

Complete contact information is available at: <https://pubs.acs.org/10.1021/acsami.0c03069>

Notes

The authors declare no competing financial interest.

ACKNOWLEDGMENTS

E.D. and C.F.-D are researchers at Centre National de la Recherche Scientifique (CNRS). M.C. is a researcher at Institut National pour la Recherche Agronomique (INRA). C.L. is an Associate-Professor at INSA de Toulouse. I.D.'s PhD is funded by MESR (Doctoral School MEGEP). I.D. thanks the technical team at LAAS, particularly, Charline Blatché and Sandrine Souleille for their help in all experiments.

REFERENCES

- (1) Drake, S. L.; Sandstedt, S. A.; Koomey, M. PilP, a Pilus Biogenesis Lipoprotein in *Neisseria Gonorrhoeae*, Affects Expression of PilQ as a High-Molecular-Mass Multimer. *Mol. Microbiol.* **1997**, *23*, 657–668.
- (2) Andersson, M.; Fällman, E.; Uhlin, B. E.; Axner, O. Dynamic Force Spectroscopy of *E. Coli* Pili. *Biophys. J.* **2006**, *91*, 2717–2725.
- (3) Lu, S.; Giuliani, M.; Harvey, H.; Burrows, L. L.; Wickham, R. A.; Dutcher, J. R. Nanoscale Pulling of Type IV Pili Reveals Their Flexibility and Adhesion to Surfaces over Extended Lengths of the Pili. *Biophys. J.* **2015**, *108*, 2865–2875.
- (4) Craig, L.; Pique, M. E.; Tainer, J. A. Type IV Pilus Structure and Bacterial Pathogenicity. *Nat. Rev. Microbiol.* **2004**, *2*, 363–378.
- (5) Telford, J. L.; Barocchi, M. A.; Margarit, I.; Rappuoli, R.; Grandi, G. Pili in Gram-Positive Pathogens. *Nat. Rev. Microbiol.* **2006**, *4*, 509–519.
- (6) Murphy, E. C.; Janulczyk, R.; Karlsson, C.; Mörgelin, M.; Frick, I.-M. Identification of Pili on the Surface of *Finexgordia Magna*—a Gram-Positive Anaerobic Cocci. *Anaerobe* **2014**, *27*, 40–49.
- (7) Krishnan, V. Pilins in Gram-Positive Bacteria: A Structural Perspective. *IUBMB Life* **2015**, *67*, 533–543.
- (8) Yanagawa, R.; Shinagawa, M. Characteristics of *Corynebacterium Renale* Phage. *Jpn. J. Vet. Res.* **1968**, *16*, 137–143.
- (9) Ton-That, H.; Schneewind, O. Assembly of Pili on the Surface of *Corynebacterium Diphtheriae*. *Mol. Microbiol.* **2003**, *50*, 1429–1438.
- (10) Hendrickx, A. P. A.; Budzik, J. M.; Oh, S.-Y.; Schneewind, O. Architects at the Bacterial Surface — Sortases and the Assembly of Pili with Isopeptide Bonds. *Nat. Rev. Microbiol.* **2011**, *9*, 166–176.
- (11) Wang, Y.; Wang, J.; Dai, W. Use of GFP to Trace the Colonization of *Lactococcus Lactis* WH-C1 in the Gastrointestinal Tract of Mice. *J. Microbiol. Methods* **2011**, *86*, 390–392.
- (12) Lebeer, S.; Claes, I.; Tytgat, H. L. P.; Verhoeven, T. L. A.; Marien, E.; von Ossowski, I.; Reunanen, J.; Palva, A.; de Vos, W. M.; de Keersmaecker, S. C. J.; Vanderleyden, J. Functional Analysis of *Lactobacillus Rhamnosus* GG Pili in Relation to Adhesion and Immunomodulatory Interactions with Intestinal Epithelial Cells. *Appl. Environ. Microbiol.* **2012**, *78*, 185–193.
- (13) Kankainen, M.; Paulin, L.; Tynkkynen, S.; von Ossowski, I.; Reunanen, J.; Partanen, P.; Satokari, R.; Vesterlund, S.; Hendrickx, A. P. A.; Lebeer, S.; De Keersmaecker, S. C. J.; Vanderleyden, J.; Hämäläinen, T.; Laukkanen, S.; Salovuori, N.; Ritari, J.; Alatalo, E.; Korpela, R.; Mattila-Sandholm, T.; Lassig, A.; Hatakka, K.; Kinnunen, K. T.; Karjalainen, H.; Saxelin, M.; Laakso, K.; Surakka, A.; Palva, A.; Salusjärvi, T.; Auvinen, P.; de Vos, W. M. Comparative Genomic Analysis of *Lactobacillus Rhamnosus* GG Reveals Pili Containing a Human- Mucus Binding Protein. *Proc. Natl. Acad. Sci. U. S. A.* **2009**, *106*, 17193–17198.
- (14) Tripathi, P.; Beaussart, A.; Alsteens, D.; Dupres, V.; Claes, I.; von Ossowski, I.; de Vos, W. M.; Palva, A.; Lebeer, S.; Vanderleyden, J.; Dufrene, Y. F. Adhesion and Nanomechanics of Pili from the Probiotic *Lactobacillus Rhamnosus* GG. *ACS Nano* **2013**, *7*, 3685–3697.
- (15) Turroni, F.; Serafini, F.; Mangifesta, M.; Arioli, S.; Mora, D.; van Sinderen, D.; Ventura, M. Expression of Sortase-Dependent Pili of *Bifidobacterium Bifidum* PRL2010 in Response to Environmental Gut Conditions. *FEMS Microbiol. Lett.* **2014**, *357*, 23–33.
- (16) Oxaran, V.; Ledue-Clier, F.; Dieye, Y.; Herry, J.-M.; Péchoux, C.; Meylheuc, T.; Briandet, R.; Juillard, V.; Piard, J.-C. Pilus Biogenesis in *Lactococcus Lactis*: Molecular Characterization and Role in Aggregation and Biofilm Formation. *PLoS One* **2012**, *7*, No. e50989.
- (17) Madsen, K.; Cornish, A.; Soper, P.; McKaigney, C.; Jijon, H.; Yachimec, C.; Doyle, J.; Jewell, L.; De Simone, C. Probiotic Bacteria Enhance Murine and Human Intestinal Epithelial Barrier Function. *Gastroenterology* **2001**, *121*, 580–591.
- (18) Wells, J. Mucosal Vaccination and Therapy with Genetically Modified Lactic Acid Bacteria. *Annu. Rev. Food Sci. Technol.* **2011**, *2*, 423–445.
- (19) Veiga, P.; Pons, N.; Agrawal, A.; Oozeer, R.; Guyonnet, D.; Brazeilles, R.; Faurie, J.-M.; van Hylckama Vlieg, J. E. T.; Houghton, L. A.; Whorwell, P. J.; Ehrlich, S. D.; Kennedy, S. P. Changes of the Human Gut Microbiome Induced by a Fermented Milk Product. *Sci. Rep.* **2014**, *4*, 6328.
- (20) Castelain, M.; Duviau, M.-P.; Oxaran, V.; Schmitz, P.; Coccagn-Bousquet, M.; Loubière, P.; Piard, J.-C.; Mercier-Bonin, M. Oligomerized Backbone Piliin Helps Piliated *Lactococcus Lactis* to Withstand Shear Flow. *Biofouling* **2016**, *32*, 911–923.
- (21) Castelain, M.; Duviau, M.-P.; Canette, A.; Schmitz, P.; Loubière, P.; Coccagn-Bousquet, M.; Piard, J.-C.; Mercier-Bonin, M. The Nanomechanical Properties of *Lactococcus Lactis* Pili Are Conditioned by the Polymerized Backbone Piliin. *PLoS One* **2016**, *11*, No. e0152053.
- (22) Meyrand, M.; Guillot, A.; Goin, M.; Furlan, S.; Armalyte, J.; Kulakauskas, S.; Cortes-Perez, N. G.; Thomas, G.; Chat, S.; Péchoux, C.; Dupres, V.; Hols, P.; Dufrene, Y. F.; Trugnan, G.; Chapot-Chartier, M.-P. Surface Proteome Analysis of a Natural Isolate of *Lactococcus Lactis* Reveals the Presence of Pili Able to Bind Human Intestinal Epithelial Cells. *Mol. Cell. Proteomics* **2013**, *12*, 3935–3947.
- (23) Le, D. T. L.; Tran, T.-L.; Duviau, M.-P.; Meyrand, M.; Guéardel, Y.; Castelain, M.; Loubière, P.; Chapot-Chartier, M.-P.; Dague, E.; Mercier-Bonin, M. Unraveling the Role of Surface Mucus-Binding Protein and Pili in Muco-Adhesion of *Lactococcus Lactis*. *PLoS One* **2013**, *8*, No. e79850.
- (24) Florin, E. L.; Moy, V. T.; Gaub, H. E. Adhesion Forces between Individual Ligand-Receptor Pairs. *Science* **1994**, *264*, 415–417.

- (25) Bowen, W. R.; Lovitt, R. W.; Wright, C. J. Atomic Force Microscopy Study of the Adhesion of *Saccharomyces Cerevisiae*. *J. Colloid Interface Sci.* **2001**, *237*, 54–61.
- (26) Dague, E.; Le, D. T. L.; Zanna, S.; Marcus, P.; Loubière, P.; Mercier-Bonin, M. Probing In Vitro Interactions between *Lactococcus Lactis* and Mucins Using AFM. *Langmuir* **2010**, *26*, 11010–11017.
- (27) Boekhorst, J.; Helmer, Q.; Kleerebezem, M.; Siezen, R. J. Comparative Analysis of Proteins with a Mucus-Binding Domain Found Exclusively in Lactic Acid Bacteria. *Microbiology* **2006**, *152*, 273–280.
- (28) Juge, N. Microbial Adhesins to Gastrointestinal Mucus. *Trends Microbiol.* **2012**, *20*, 30–39.
- (29) Mercier-Bonin, M.; Chapot-Chartier, M.-P. Surface Proteins of *Lactococcus Lactis*: Bacterial Resources for Muco-Adhesion in the Gastrointestinal Tract. *Front. Microbiol.* **2017**, *8*, 2247.
- (30) Otto, M. Staphylococcal Biofilms. *Curr. Top. Microbiol. Immunol.* **2008**, *322*, 207–228.
- (31) Hutter, J. L.; Bechhoefer, J. Calibration of Atomic-force Microscope Tips. *Rev. Sci. Instrum.* **1993**, *64*, 1868–1873.
- (32) Benoit, M.; Gabriel, D.; Gerisch, G.; Gaub, H. E. Discrete Interactions in Cell Adhesion Measured by Single-Molecule Force Spectroscopy. *Nat. Cell Biol.* **2000**, *2*, 313–317.
- (33) Beaussart, A.; Herman, P.; El-Kirat-Chatel, S.; Lipke, P. N.; Kucharíková, S.; Van Dijck, P.; Dufrière, Y. F. Single-Cell Force Spectroscopy of the Medically Important *Staphylococcus Epidermidis*-*Candida Albicans* Interaction. *Nanoscale* **2013**, *5*, 10894–10900.
- (34) Bustamante, C.; Marko, J. F.; Siggia, E. D.; Smith, S. Entropic Elasticity of Lambda-Phage DNA. *Science* **1994**, *265*, 1599–1600.
- (35) Janshoff, A.; Neitzert, M.; Oberdörfer, Y.; Fuchs, H. Force Spectroscopy of Molecular Systems—Single Molecule Spectroscopy of Polymers and Biomolecules. *Angewandte Chemie International Edition* **2000**, *39*, 3212–3237.
- (36) Francius, G.; Lebeer, S.; Alsteens, D.; Wildling, L.; Gruber, H. J.; Hols, P.; De Keersmaecker, S.; Vanderleyden, J.; Dufrière, Y. F. Detection, Localization, and Conformational Analysis of Single Polysaccharide Molecules on Live Bacteria. *ACS Nano* **2008**, *2*, 1921–1929.
- (37) Kline, K. A.; Kau, A. L.; Chen, S. L.; Lim, A.; Pinkner, J. S.; Rosch, J.; Nallapareddy, S. R.; Murray, B. E.; Henriques-Normark, B.; Beatty, W.; Caparon, M. G.; Hultgren, S. J. Mechanism for Sortase Localization and the Role of Sortase Localization in Efficient Pilus Assembly in *Enterococcus Faecalis*. *J. Bacteriol.* **2009**, *191*, 3237–3247.
- (38) de Weirdt, R.; de Wiele, T. V. Micromanagement in the Gut: Microenvironmental Factors Govern Colon Mucosal Biofilm Structure and Functionality. *npj Biofilms Microbiomes* **2015**, *1*, 15026.
- (39) Piard, J.-C.; Briandet, R. Lactic Acid Bacteria Biofilms. In *Biotechnology of Lactic Acid Bacteria*; John Wiley & Sons, Ltd, 2015; pp 341–361, DOI: 10.1002/9781118868386.ch20.
- (40) Wang, H.; Wilksch, J. J.; Chen, L.; Tan, J. W. H.; Strugnell, R. A.; Gee, M. L. Influence of Fimbriae on Bacterial Adhesion and Viscoelasticity and Correlations of the Two Properties with Biofilm Formation. *Langmuir* **2016**, *33*, 100–106.
- (41) Burgain, J.; Scher, J.; Lebeer, S.; Vanderleyden, J.; Cailliez-Grimal, C.; Corgneau, M.; Francius, G.; Gaiani, C. Significance of Bacterial Surface Molecules Interactions with Milk Proteins to Enhance Microencapsulation of *Lactobacillus Rhamnosus* GG. *Food Hydrocolloids* **2014**, *41*, 60–70.
- (42) Guerin, J.; Bacharouche, J.; Burgain, J.; Lebeer, S.; Francius, G.; Borges, F.; Scher, J.; Gaiani, C. Pili of *Lactobacillus rhamnosus* GG Mediate Interaction with β -Lactoglobulin. *Food hydrocolloids* **2016**, *58*, 35–41.
- (43) Fahs, A.; Quilès, F.; Jamal, D.; Humbert, F.; Francius, G. In Situ Analysis of Bacterial Extracellular Polymeric Substances from a *Pseudomonas Fluorescens* Biofilm by Combined Vibrational and Single Molecule Force Spectroscopies. *J. Phys. Chem. B* **2014**, *118*, 6702–6713.
- (44) Miller, E.; Garcia, T.; Hultgren, S.; Oberhauser, A. F. The Mechanical Properties of *E. Coli* Type 1 Pili Measured by Atomic Force Microscopy Techniques. *Biophys. J.* **2006**, *91*, 3848–3856.
- (45) Huang, Q.; Wu, H.; Cai, P.; Fein, J. B.; Chen, W. Atomic Force Microscopy Measurements of Bacterial Adhesion and Biofilm Formation onto Clay-Sized Particles. *Sci. Rep.* **2015**, *5*, 16857.
- (46) Rheinlaender, J.; Gräbner, A.; Ott, L.; Burkovski, A.; Schäffer, T. E. Contour and Persistence Length of *Corynebacterium Diphtheriae* Pili by Atomic Force Microscopy. *Eur. Biophys. J.* **2012**, *41*, 561–570.